GeoConvention
Calgary • Canada • March 7-11 2016
OPTIMIZING RESOURCES

# Signal to noise analysis of densely sampled microseismic data

*Konrad Cieslik and Brad Artman*, Spectraseis Inc., Steve Roche and Jason Gumble, Cimarex Energy*

## Summary

The signal to noise ratio improvement due to noise cancelation inherent in stacking individual measurements is bounded by the square root of the number of channels stacked. Due to the non-impulsive radiation pattern of microseismic arrivals and local noise sources within an array, this upper limit is impossible to achieve. This study uses a densely sampled array designed for a 3D converted-wave reflection experiment to analyze the actual signal to noise ratio improvement as a function of channel count. After several hundred stations, the return on acquisition investment is minimal. Shear arrivals are more energetic than compression arrivals. The combination of both types of information makes a further improvement of available energy for each event. Shear arrivals often have low dominant frequency content. This example shows arrivals below the corner frequency of the hardware, which results in a lower signal to noise ratio than if broadband instruments were used. If sparse and/or irregular acquisition patterns do not evenly sample the radiation pattern, no benefits or even deleterious effects can be observed on the information content.

## Introduction

The fundamental problem of geophysical processing of microseismic data is an approximate deconvolution of the convolution of source, earth, and acquisition parameters that result in the wavefields we record. First we must acknowledge that the microseismic wavefield, with its non-impulsive radiation patterns, are fundamentally different from the wave fields that the reflection seismic community has been deftly exploiting for many decades. We must keep in mind the impulse response of our antennae, and how consistently we measure signal throughout a large earth volume along long horizontal well bores and multi-well pads.

In this paper, we capitalize on an 8x8 km 3C array to investigate the information content of the wave-field as a function of channel count and arrival modes. While the array was designed for a converted wave reflection seismic experiment, two horizontal wells were stimulated beneath it and collected microseismic arrivals. The array has nodal 3C geophones with 10 Hz corner frequency deployed every 50 m inline, with a 352 m cross-line interval adding to approximately 3000 stations. Two arrivals from this acquisition are used to investigate the signal to noise increase as a function of the number of stations stacked after move-out correction.

## Data set

Figure 1 shows the aligned data traces from a strong event in the catalog. No geophysical (migration) processing was performed in this instance, only correlation-based time shifts and polarity corrections. This resulted in a single-sample precision of the time shifts. Figure 2 is a map view of the polarity of the arrivals extracted after flattening and rotating Z,N,E components into the compressional, and radial and transverse shear coordinate system. The common color map used for all arrivals shows, as expected (Aki and Richards, 2002), that the two shear arrivals are significantly more energetic than the P arrival. Also as expected, that the Sv, or radial, mode has the same radiation pattern as the P arrival. With the array centered over two wells being investigated, the aperture in the NE quadrant is slightly insufficient for this event from the Eastern well.

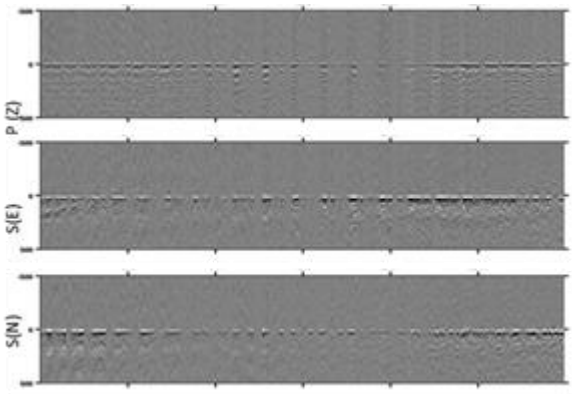


Figure 1: Time-aligned data traces showing a strong microseismic arrival.

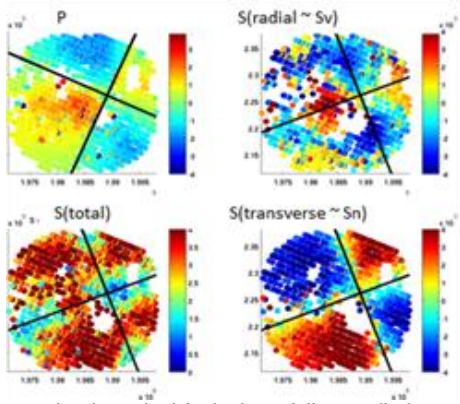


Figure 2: Text-book vertical-fault shear failure radiation pattern with fault and auxilliary planes superimposed in black. Color scales are constant among all panels.

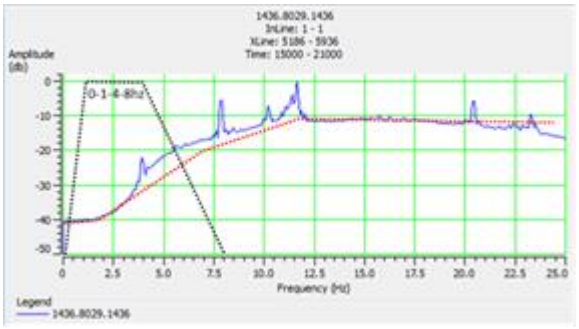


Figure 3: PSD energy plot of the shear arrival on one horizontal component and the approximate noise level of the geophone-amplifier.

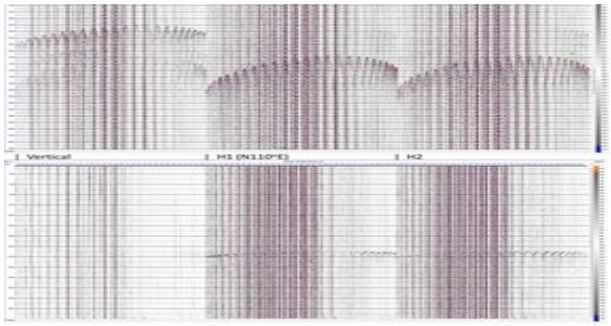

Figure 4: 30 s of broad spectrum data (top) showing clear P and S arrivals. And after the low-frequency pass depicted in Figure 3, the P wave has been removed.

Figure 3 shows the power spectral density (PSD) analysis of the event. The red dashed line is the interpreted noise floor of the sensor-amplifier system showing the roll-off in sensitivity of the geophones below their natural frequency. The distance between the blue data PSD and the red system response represents the signal to noise ratio of the shear arrival on this horizontal component. The information content of this mode is between ~ 3-12 Hz, and being attenuated across this entire band by the 10 Hz geophone.

Figure 4 shows the data traces of the P and S arrivals before and after the low-frequency pass band depicted by the trapezoid in Figure 3. Interpreting Figures 2-4 together, it is clear that the shear arrival is lower frequency and more energetic than the P (Witten et al. 2012), insomuch as it is even recordable despite the high frequency equipment fielded (Dellinger et al., 2009).

## Signal to noise ratio

The quality of, and therefore the ease of use of a data set, is defined by the signal to noise ratio of the information in the records (Drew et al., 2014). While advanced signal processing and migration methods help extend the usefulness of a data volume, the total information content is defined by the signal to noise ratio. For this exploration, we define the signal to noise ratio after stack rather than on single traces. While we did not perform a true migration, the correlation-based alignment and polarity corrections result in an image-domain measure. We present the stacking results using balanced traces, which partially compensates for the amplitude variation on traces within the array. This then represents a best-case scenario for microseismic stacking, since stacking theory assumes unit contribution of every extra measurement (Wikipedia, 2014, Sheriff, 2011), while variability and zeroes are the reality in this

context. Our noise energy was measured from the previous 10 s of data before the arrival. Figure 5 shows energy in dB as the channels stacked from Figure 1 are added. We simply stack the data from the SW to the NE along acquisition lines, thus ignoring the radiation pattern details. As the lines cross nodal planes and amplitude variations in the radiation pattern, we find a non-monotonic function.

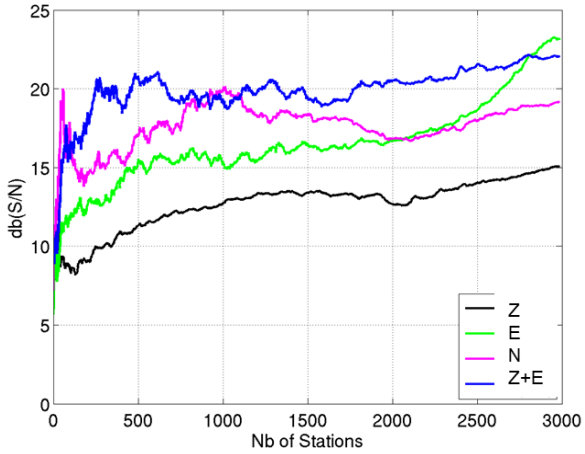


Figure 5: Signal to noise energy functions with increasing channel count stacking along acquisition lines.

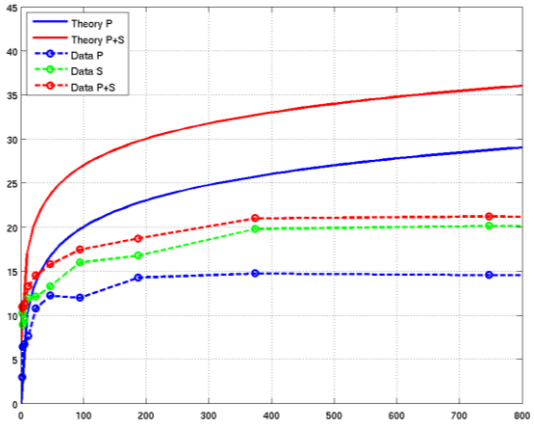


Figure 6: Stacking function of first 800 regularly sampled full aperture stations. Solid lines are theoretic square root functions, while dashed lines are those measured with this event.

However, if we maintain the regular sampling of the arrivals across the whole aperture of the array and increase sampling interval instead, we do find a more reasonable monotonic and asymptotic increase in signal to noise ratio with increasing channels. Figure 6 shows the stacking functions generated from a full-footprint decimation exercise of the array, only extending through the first 800 channels as the asymptotic nature of the function has already developed.

The solid lines show the theoretical stacking curves that are simple functions of the square root of channels (Wikipedia, 2014). The blue line assumes unit amplitude of a hypothetical P wave arrival on every station. The red curve is the result of summing the P arrival and a hypothetical S arrival that is only two times higher amplitude than the P. This assumption is highly conservative (Aki and Richards, 2002), but results in about a 5 dB increase in S/N if both modes are used instead of only the P. As expected, the real data calculations fall below the best-case scenario of stacking theory.

The dashed curves show the measured full-footprint stacking curves from the data in Figures 1 and 2. The blue curve is the P arrival only taken from only the vertical component geophone so as to compare directly to a single component acquisition. It is clear from the top panel of Figure 4 that there is substantial energy from all modes on every orthogonal component. The rotation into source/mode coordinates as shown in Figure 2 removes this cross-talk. The green curve is the energy function for only the two S arrivals, while the red curve is the sum of both P and S energy. Again we find a systematic +7 dB of information when we use all wave arrivals for an event.

Figures 5 and 6 show a total information content of about 15 dB for the P arrival. This S/N ratio is reached by 400 stations, and is only 2 dB less at 200 stations. The 15 dB level is reached using the shear information even earlier.

Figure 7 shows a much weaker microseismic event. We perform the same processing and analysis for this event as described above for the stronger event above. Figure 8 shows the zoomed in view of regularly decimated S/N ratio response to increasing channel count for the weak event in Figure 7. The analytical curves (solid lines) are the same as those in Figure 6. In the figures, we find again that the pattern of S/N increase does follow the theoretical function, but is substantially less energetic than the stronger event above.

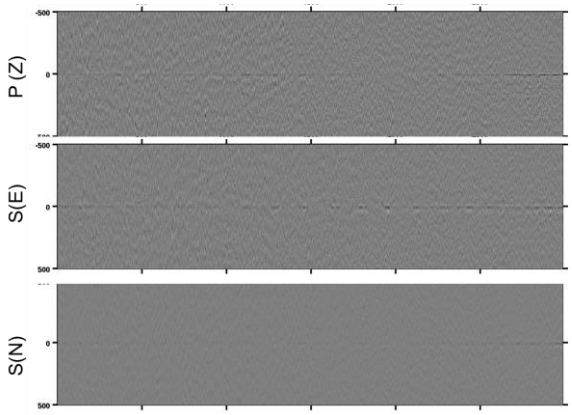


Figure 7: Time-aligned data traces for weak event.

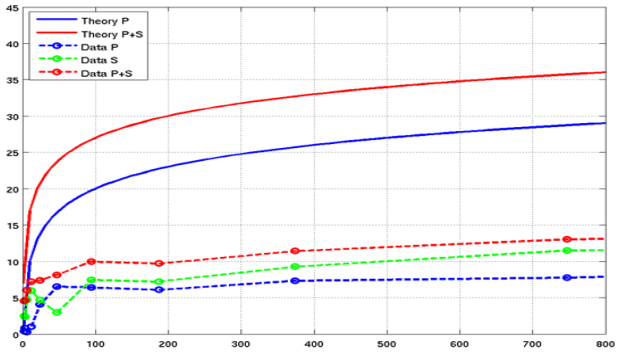


Figure 8: Stacking function of first 800 regularly sampled full aperture stations from Figure 7 showing assymptotic limits. Solid lines are theoretic square root functions, while dashed lines are those measured with this event.

## Discussion

The stacking curves as presented for this single event are representative of all events of different size. As events get weaker, the curves shift down the energy axis, but retain their shapes as expected. The curves become quite irregular as the S/N ratio at the trace level makes precise time shifts, amplitude extractions, and polarity corrections less accurate.

The standard geophones with 10 Hz corner frequency are able to record strong low frequency arrivals as long as they are more energetic than the damping in the system would attenuate. The frequency content of the arrivals suggests that a broadband instrument would enjoy an even better S/N ratio for the S arrivals. This assumption leads one to interpret the shear wave stacking curves as a pessimistic minimum due to measurement peculiarities rather than actual wave-field energy content.

## Conclusion

The signal to noise ratio improvement due to noise cancelation inherent in stacking individual measurements for real data is bounded by the square root of the number of channels stacked, not equal to the theoretical function. The theoretical function assumes that each channel contributes equally to the signal, and that noise is perfectly Gaussian random energy. The first assumption is specifically violated for microseismic arrivals that have radiation patterns. The second assumption is usually violated in real field work.

As physics dictates, the S waves are systematically more energetic than the P waves. The S waves are systematically lower frequency events than the P waves. The 10 Hz geophones attenuated a substantial portion of the S arrivals, so we expect the energy curves shown to be a lower limit to the realities of the wavefield that are different to the content of the records. Also, we applied the same bandpass (2-60 Hz) for all data channels for consistency, which does not take into account the different frequency bands of the different arrival modes resulting in slightly lower S/N ratio for all. However, using both P and S arrivals for a single event returns substantial value with fewer stations compared to single component recording.

Both strong and weak events adhere to power-law increase in S/N ratio. However, monotonic increases are only observed when the footprint of the array covers the entire, or at least most of the, radiation pattern. Sparse lines or patches that do not evenly sample the radiation may actually suffer in the S/N domain by adding stations in or near nodal planes.

With this oversampled microseismic data set we had the opportunity to calculate empirically, without any assumptions, the S/N increase with increasing channel count for both P and S waves. These observations allow more grounded conversations around the value return (S/N ratio energy) for incremental acquisition expense.

## References


Aki, K., and P. Richards, 2002, Quantatitive Seismology: University Science Books.

Dellinger, J., B. P. America, John Blum, and Meredith Nettles (2009) The 10 February 2006 “Green Canyon” earthquake: A case history of an unusual seismic event. SEG Technical Program Expanded Abstracts 2009: pp. 572-576. doi: 10.1190/1.3255822

Drew, J., Paolo Primiero, Keith Brook, Daniel Raymer, Tony Probert, Ahyi Kim, and David Leslie (2012) Microseismic monitoring field test using surface, shallow grid, and downhole arrays. SEG Technical Program Expanded Abstracts 2012: pp. 1-5. doi: 10.1190/segam2012-0910.1

Drew, J., Jian Zhang, and Joel Le Calvez (2014) The impact of channel count on microseismic event detection for a surface array. SEG Technical Program Expanded Abstracts 2014: pp. 2183-2187. doi: 10.1190/segam2014-1377.1

Estelle Schisselé-Rebel and Julien Meunier (2013) Patch versus broadband networks for microseismic: A signal-to-noise ratio analysis. SEG Technical Program Expanded Abstracts 2013: pp. 2104-2108. doi: 10.1190/segam2013-1285.1

Sheriff, R.E. [2011] Encyclopedic Dictionary of Applied Geophysics. 4th Edition. Society of Exploration Geophysicists, Tulsa, USA.

Witten, B., Summer Montgomery, and Brad Artman (2012) Shear wave arrivals in surface microseismic data. SEG Technical Program Expanded Abstracts 2012: pp. 1-5. doi: 10.1190/segam2012-0722.1

Wikipedia contributors (2014) Signal averaging, Wikipedia, The Free Encyclopedia, http://en.wikipedia.org/w/index.php?title=Signal_averaging&oldid=630620714 (accessed April 1, 2015).